Applied Surface Science 702 (2025) 163294

Contents lists available at ScienceDirect

Applied Surface Science

journal homepage: www.elsevier.com/locate/apsusc

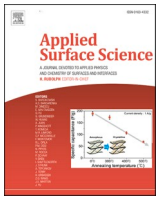

Full Length Article

A high-resolution core level spectroscopy study of Ir: From flat to reconstructed and stepped surfaces

Deborah Perco [a], Monica Pozzo [b,c], Andrea Berti [a], Paolo Lacovig [d], Marco Bianchi [d], Silvano Lizzit [d], Dario Alfè [e,f], Alessandro Baraldi [a,d,*]

[a] Department of Physics, University of Trieste, Via Valerio 2, 34127 Trieste, Italy
[b] Faculty of Technological & Innovation Sciences, Universitas Mercatorum, Piazza Mattei 10, 00186 Rome, Italy
[c] Institute for Materials Discovery, UCL East, Marshgate Building, 7 Sidings Street, Stratford, London E20 2AE, the United Kingdom of Great Britain and Northern Ireland
[d] Elettra - Sincrotrone Trieste, AREA Science Park, S.S. Km 163.5 Basovizza, 34149 Trieste, Italy
[e] Department of Earth Sciences and London Centre for Nanotechnology, University College London, Gower Street, London WC1E 6BT, the United Kingdom of Great Britain and Northern Ireland
[f] Dipartimento di Fisica Ettore Pancini, Università di Napoli Federico II, Monte S. Angelo, 80126 Napoli, Italy

ARTICLE INFO

Keywords:
Ir
Iridium
XPS
DFT
Low coordination
Under-coordinated atoms
D-band centre
Chemical reactivity

ABSTRACT

The ability to distinguish surface atoms with different coordination numbers is of fundamental importance in many fields of materials science, ranging from magnetism to heterogeneous catalysis. In this study, we exploited the capability of high-resolution core-level photoelectron spectroscopy in combination with density functional theory-based calculations to investigate this kind of atomic configurations. The measurement of the $4f_{7/2}$ core level of the (111), (100), (110), (311), and (510) surfaces allowed us to highlight the differences between surface atoms with different coordination, also related to surface reconstruction processes, atomic diffusion, and morphological changes. The shifts in core levels were correlated with the modification of the effective coordination number, which takes into account the role of the variability in the Ir-Ir interatomic distances, and with the variations in the centroids of the projected d-band ΔB_d, a quantity in turn related to chemical reactivity. Besides solid surfaces, the results may aid in understanding the properties of Ir nanoparticles whose active sites on nanofacets, such as edges, corners, and steps, are of paramount relevance in heterogeneous catalysis, especially in the electrocatalytic oxygen evolution reaction.

1. Introduction

The concept of low-coordinated atoms has become increasingly important in various fields of materials science. Numerous studies have highlighted the enhanced chemical reactivity of nanoparticles exhibiting nanofacets with high Miller indexes. These nanofacets are characterized by atoms with a coordination number n lower than that typically found on "closed-packed" surfaces ($n = 9$ for fcc(111) and hcp(0001); $n = 8$ for fcc(100); $n = 7$ for fcc(110)) [1,2]. Over the past 15 years, new synthesis methods and strategies have been developed, enabling precise control over nanocrystal morphology [3,4], which in turn imparts unique chemical properties.

However, one inherent challenge in this approach is the stability of low-coordinated atoms. Due to their reduced number of bonds, these atoms are prone to displacement from their atomic positions under thermal excitation, which is common at the temperatures of typical catalytic reactions. As a result, they exhibit large surface mobility, migrating to lower-energy configurations with higher coordination numbers. This process ultimately can lead to particle coarsening and the formation of larger agglomerates as their size increases [5]. A particularly relevant example is the diffusion of single adatoms across nanofacets on a catalyst [6]. The migration process is often influenced by reaction conditions, particularly the presence of adsorbates such as hydrogen, oxygen, and carbon monoxide, which can increase the mobility of these adatoms [7]. One of the main challenges in this field is identifying and determining the physical and chemical properties of these atoms. In this regard, in addition to atomic-resolution microscopy-based techniques such as Transmission Electron Microscopy (TEM) and Scanning Tunneling Microscopy (STM), core-level Photoelectron Spectroscopy has proven to be a powerful tool for distinguishing surface

* Corresponding author.
E-mail address: alessandro.baraldi@elettra.eu (A. Baraldi).

https://doi.org/10.1016/j.apsusc.2025.163294
Received 26 February 2025; Received in revised form 12 April 2025; Accepted 16 April 2025
Available online 17 April 2025

atoms in different chemical environments [8,9]. In this work, we employed this spectroscopic approach to study a set of single crystal iridium surfaces, each formed by atoms with different local configurations and atomic coordination in their first layers. Despite its increasing cost (+229 % from 2018 to 2021 [10]), iridium continues to play a crucial role in many areas of heterogeneous catalysis and electrochemistry, both in its metallic, alloy and oxide forms for its high activity and durability in nanoscale Oxygen Revolution Reaction catalysts and in photocatalysis [11,12].

Our comparative study of the Ir $4f_{7/2}$ core levels of (111), (100), (110), (510) and (311) iridium surfaces revealed differences that are important in identifying the presence of different local atom configurations, whose features can be linked to chemical reaction properties relevant to heterogeneous catalysis. These surface terminations were selected based on their geometric structures. The (111) surface, which has the highest atomic packing and lowest free energy, is widely studied in the field of catalysis and as a support to probe the properties of 2D materials [13]. The Ir(110) surface is known for its atomic reconstruction, forming troughs along the [1$\bar{1}$0] direction with (1 × 2), (1x3) and (1 × 4) periodicities [14,15]. Also the Ir(100) surface undergoes reconstruction, resulting in a highly corrugated quasi-hexagonal layer with a (1 × 5) periodicity [16–20], where six Ir rows are arranged in a close-packed fashion on top of five rows of the square substrate. The reduction of the coordination is the driving force for the formation of this quasi-hexagonal reconstruction in the so-called "buckled-two-bridge" model, where the registry between the first atomic layer and the substrate underneath is defined via the occupation of two bridge sites and results in a strong strain field which stabilizes the reconstruction. The (311) and (510) surfaces are stepped crystallographic terminations. The Ir(311) surface, although recognized as an "open" surface, is energetically quite stable. It results from significant atomic motion during the oxygen-induced faceting of the Ir(210) surface [21]. In this specific case the atomic diffusion process leads to the formation of triangular nanopyramids, whose sides are formed by the [311] and [31$\bar{1}$] planes, along with [110] nanofacets. In this context, the crystallographic plane orientation is expected to play a key role even in the formation of IrO_2 nanoparticles, which have also been extensively studied using X-ray photoelectron spectroscopy [22,23]. Interestingly, in contrast to the (111), (100), and (110) low Miller index surfaces, the (311) fcc surface provides only a mirror plane, offering a bonding site that allows for the formation of long-range self-organizing chirality, similar to that observed on copper [24]. The (510) surface, with its 5-atoms terraces oriented along the (100) plane and (111) steps, is also known for producing non-linear catalytic behavior [25], due to periodic processes of adsorbate-induced lifting of surface reconstruction.

2. Methods

2.1. Experimental methods

High-resolution core level spectroscopy (HR-CLS) experiments were carried out at the SuperESCA beamline of the Elettra synchrotron radiation facility. The measurement chamber is equipped with a SPECS 150 electron energy analyzer, provided with a delay line detector developed in house, Low Energy Electron Diffraction (LEED) and a mass spectrometer. The beamline provides photons between with energy ranging from 100 to 1500 eV with a resolving power of 10^4 at 400 eV. Among the different surfaces, (110) and (100) surfaces were instead measured using a double pass hemispherical electron energy analyser (mean radius 150 mm) [26].

All the Ir surfaces were typically cleaned by repeated cycles of Ar^+ bombardment followed by annealing up to 1350 K and oxygen exposure ($p = 5 \times 10^{-8}$ mbar) and a final reduction in hydrogen ($p = 1$ x 10^{-7} mbar), until no impurities (C, S, Si and B in particular) were detected by XPS within the detection limit (0.1 % ML, where 1 ML corresponds to 1.56x10^{15} atoms/cm^2 for Ir(111)). It is important to underline that the oxygen treatment, employed to remove the little amount of C contamination, is a procedure that was not always adopted in the past to clean the Ir surfaces.

For all surfaces the Ir $4f_{7/2}$ core level spectra were measured in the photon energy range between 130 and 200 eV, with energy resolution better than 50 meV (80 meV for Ir(110) and Ir(100)), as determined by measuring the Fermi edge width (at 12 % and 88 % of the intensity) of a Ag sputtered polycrystal, and for some surfaces at different emission angles to enhance the signal of the surface components. It is important to underline that at these photoelectron kinetic energies (in the range between about 70 and 140 eV) the effects of photoelectron diffraction can play a relevant role and therefore both azimuthal and polar emission angles are important in defining the overall intensity of each component, as widely demonstrated for a variety of surfaces [27–29]. The Ir single crystals were mounted on a liquid-nitrogen cryostat manipulator with four degrees of freedom, three translations and the polar rotation. The samples were cooled to 80 K for the measurements and heated by electron bombardment from hot tungsten filaments mounted behind them. The temperature of the samples was monitored by means of two K-type thermocouples directly spot-welded on the crystal side.

When performing HR-CLS measurements to determine surface core level shifts (SCLS), a very good background pressure is always required, since even a tiny density of impurities such as adsorbed hydrogen, water and carbon monoxide, which are typical contaminants in a ultra-high vacuum environment, may alter the line shapes and binding energies (BE) of the core-level components, as well as cause the appearance of new spectral features. This is why the pressure was always maintained below 1.5 x 10^{-10} mbar during data acquistion at 80 K, needed also to reduce the contribution of phonon-induced broadening. Anyhow every 15 min the samples were flash annealed to 670 K to induce the desorption of unwanted species from the substrate surface, such as H_2 and CO.

LEED and Spot-Profile Analysis LEED images were acquired in a second chamber at the Nanoscale Materials Laboratory at Elettra – Sincrotrone Trieste. The Omicron SPA-LEED system allows the measurement of the diffraction spots line shape, with a transfer width of the instrument which is better than 700 Å at electron kinetic energy of 115 eV. The base pressure in all ultrahigh-vacuum chambers during the experiments was always below 2×10^{-10} mbar.

All the $4f_{7/2}$ core level spectra were analysed using a Doniach-Šunjič function (DS) [30] convoluted with a Gaussian distribution, as commonly accepted for the case of metal surfaces [28,31,32]. The DS profile combines a Lorentzian width L, which is related to the finite core–hole lifetime, with the Anderson singularity index α, which reflects the occurrence of electron-hole pair excitations. The Gaussian width G accounts for phonon broadening, instrumental resolution, and any inhomogeneous broadening. The background was assumed to be linear. The reported BE positions of the spectra were calibrated with respect to the Fermi energy, which was measured under the same experimental conditions.

2.2. Theoretical methods

Calculations were performed using density functional theory with exchange–correlation effects included at the level of the rev-vdw-DF2 functional [33]. We used the Projector Augmented Wave method as implemented in VASP [34] to account for the core electrons of both Ir, with the 6s and 5d electrons explicitly included in the valence. We used a plane-wave kinetic energy cutoff of 400 eV.

The Ir(111) surface was modelled using 6 atomic layers with the three bottom layers atoms fixed at their bulk position, even though 5 layers are enough to achieve a SCLSs convergence. The (311) surface of Ir was modeled using a slab with a thickness of 8 layers, with the atoms of the bottom cell (4, 5, 6, 7 and 8 layers) kept fixed at their bulk positions, while all the other atoms were allowed to relax. A vacuum

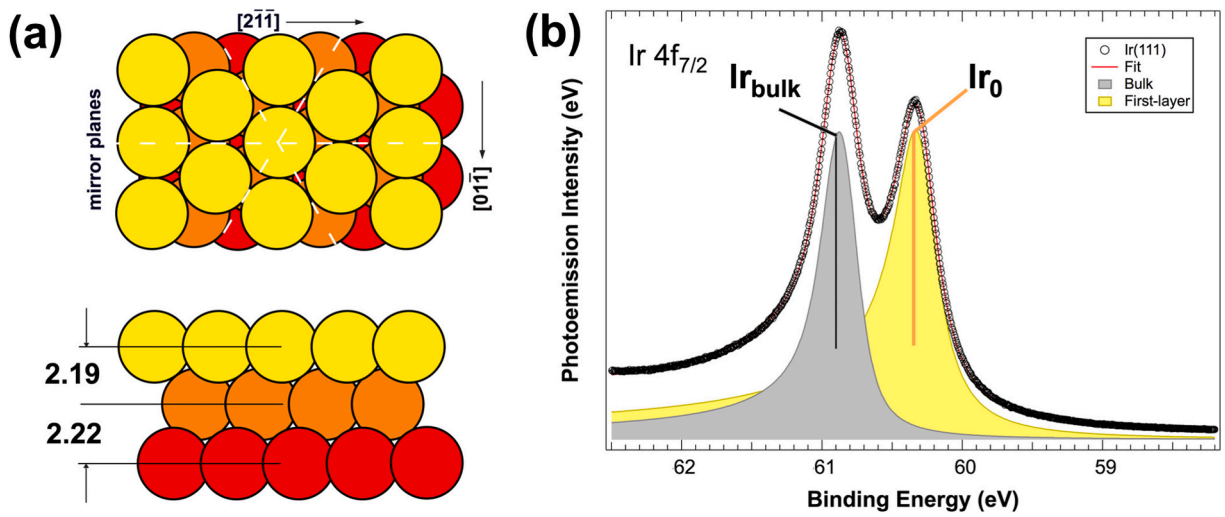

Fig. 1. DFT structure and HR-CLS of Ir(111). (a) Structural geometry in the top and side views as obtained by DFT. The values of inter-layer distances are reported in Å. (b) $4f_{7/2}$ core level spectrum measured at T = 80 K and hv = 200 eV. The grey (Ir_{bulk}) and yellow (Ir_0) peaks indicate the bulk and the clean surface component, respectively, while the red curve is the result of the fitting.

interspace of at least 19.5 Å was used to minimize the interaction between periodic images of the slab along the direction perpendicular to the surface, resulting in a supercell of 27.4 Å along the z-axis.

The (110) surface, both in the reconstructed (1x2) and (1x3) form and in its unreconstructed (1x1) geometry, were modelled using an 8 atomic layer slab, of which the upper three layers were allowed to relax while atoms in the other layers were kept fixed at their bulk position. Eventually, (100)-5x1 surface was modelled using eight layers as well with the same fixed-non fixed number of layers.

For these calculations we used a Monkhorst – Pack k-point sampling of 2 × 2 × 1 k-points. In all calculations the energy was minimized until the forces acting on the atoms were smaller than 0.03 eV/Å.

Core-electron binding energies for both bulk and surface atoms have been estimated in the so-called final-state approximation, as follows: first a standard calculation is performed on the fully relaxed system (bulk or slab). Then, in a subsequent calculation, an electron from the chosen core level of a particular atom is excited to the lowest conduction band, and the valence electronic structure is relaxed at fixed atomic configuration. The energy difference between these two calculations provides an estimate of the core level binding energy. The SCLS is then given as the difference of core binding energies between the surface and bulk atoms, i.e.

$$\mathrm{SCLS} = E_{binding}\,(\mathrm{surface}) - E_{binding}(\mathrm{bulk}) \tag{1}$$

In our case, core electrons from the 4f shell have been excited to the lowest empty band. According to previous theoretical studies, the method used in the present work to calculate the SCLSs yields an accuracy of about 20–50 meV on the results.

We also calculated the partial density of states $n^i_{lm}(E)$ of atom i, defined as the projection of the density of states onto spherical harmonics Y^i centered on the atom:

$$n^i_{lm} = \sum_n \int d\boldsymbol{k} \left|\langle Y^i_{lm} | \psi_{N\boldsymbol{k}} \rangle\right|^2 \delta(E - E_{N\boldsymbol{k}}) \tag{2}$$

with the projection $\langle Y^i | \psi \rangle$ calculated by integrating over a *lm* Nk sphere of radius $R_i = 1.42$ Å centered on atom i. Here ψ_{Nk} is the crystal wave function of band N at wave-vector k, and E_{nk} is the corresponding energy eigenvalue. We define the p^{th} moment of the density of states $n^i_{lm}(E)$ as $\mu_p = \int dE E^p n^i_{lm}(E)$; μ_0 and μ_1/μ_0 give the total number of states in the band and the band center B^{id}, respectively. In particular, we define the d-band center B^{id} of atom i as the ratio μ_1/μ_0 obtained from the partial density of states

$$n^i_d(E) = \sum_{m=-2}^{2} n^i_{2m}(E) \tag{3}$$

3. Experimental and theoretical results

3.1. Ir(111)

Ir(111) is an unreconstructed closed-packed (1x1) surface, as is evident from the LEED image presented in Supplementary Fig. S1, where it is presented with inverted contrast for better visibility. The theoretical distance between nearest neighbours atoms is 2.73 Å, with d_{12} distance between the first and second layer and d_{23} between the second and third layer being equal to 2.19 and 2.22 Å, respectively (see Fig. 1(a)), thus corresponding to a small expansion with respect to the bulk interplanar distances of + 0.35 % and + 1.72 %. The $4f_{7/2}$ spectrum of Ir(111), shown in Fig. 1(b), presents two components assigned to bulk atoms (at higher binding energy, $Ir_{bulk} = 60.84 \pm 0.02$ eV) and surface atoms (Ir_0) with a calculated core level shift of −545 meV. This finding is consistent with the theoretical predictions based on the simple-equivalent core approximation predictions [35] for a more than half-filled d-band metal, such as Iridium, which suggest that all surface features should experience BE shifts to lower values than the bulk counterpart. This value is also in excellent agreement with the results of the analysis of the experimental data, which show a shift of −550 meV, in agreement with previous findings [32,36]. The line shape parameters of the two components turned out to be different: Lorentzian and Gaussian width are equal to 0.29 eV and 0.08 eV for surface atoms, 0.17 eV and 0.08 eV for the bulk; the asymmetry parameter takes a value of 0.22 and 0.15, respectively, for first and bulk layers.

3.2. Ir(110)

The (110) surface of Ir presents several reconstructed phases of the missing-row type, namely (1x2), (1x3) and (1x4), although stabilisation effects on the macroscopic scale with the formation of (331) facets are reported when no oxygen cleaning treatment is used [37]. Recent theoretical calculations [14] showed that the three phases have a very similar energy, which is within the indeterminacy range of the theoretical approach used. The formation of these structures differentiates Ir from the case of (110) fcc surfaces of similar metals such as Pt and Au in which the surface reconstructs with a (1x2) periodicity [38,39]. The phase prepared in this work corresponds to a (1x2) obtained after

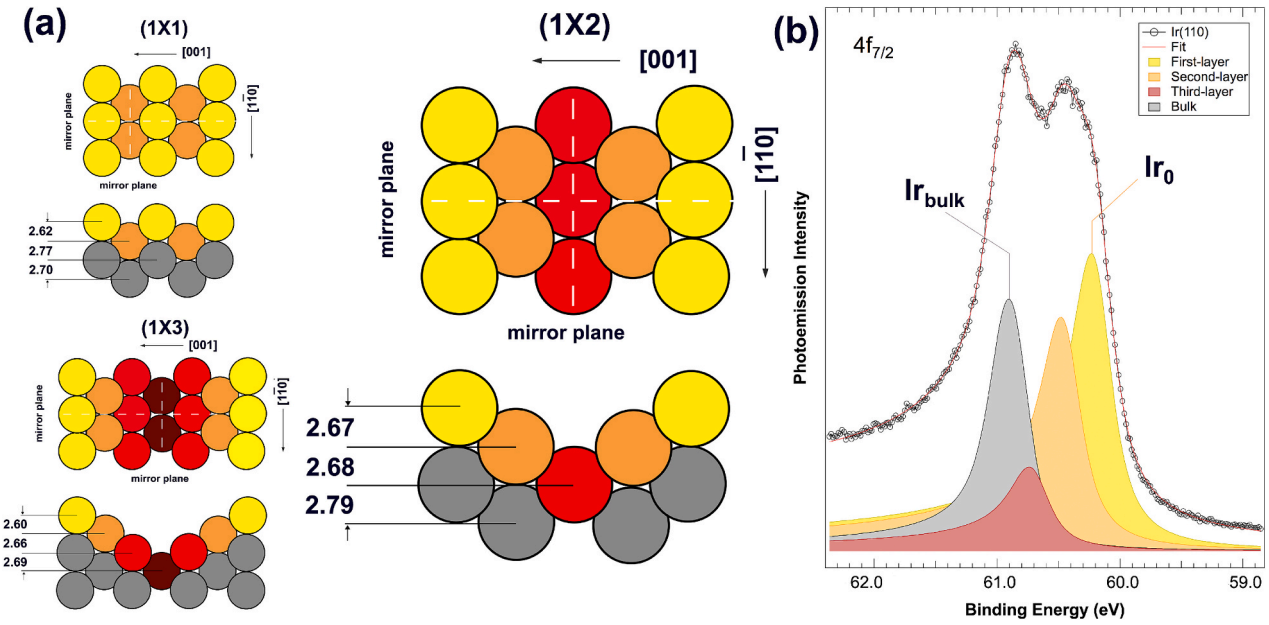

Fig. 2. DFT structures and HR-CLS of Ir(110). (a) Structural geometries of the (1x1), (1x3) and (1x2) surface reconstructions, as obtained by DFT. The (1x2) structure corresponds to the experimental LEED pattern. The values of inter-layer distances are reported in Å. (b) $4f_{7/2}$ core level spectrum measured at T = 80 K and hv = 185 eV. The grey (Ir_{bulk}), yellow (Ir_0), orange, and red peaks indicate the bulk and clean surface components, respectively, of the (1x2) missing-row structure, while the red curve is the result of the fitting.

Table 1
DFT computed and experimental core level shifts for surface atoms of (1x1), (1x2) and (1x3) Ir(110) surfaces. Error bars associated to experimental values are ± 30 meV.

	DFT (meV)				Experimental (meV)			
	Surface	2nd layer	3rd layer	4th layer	Surface	2nd layer	3rd layer	4th layer
Ir(110)-(1x1)	−770	−80	−30	–	–	–	–	–
Ir(110)-(1x2)	−690	−440	−170	–	−710	−430	−140	–
Ir(110)-(1x3)	−830	−520	−430	−110	–	–	–	–

annealing at 1070 K the sputtered surface, followed by oxygen treatment (p_{H2} = 5x10^{-8} mbar) and reduction with hydrogen (p_{H2} = 1x10^{-7} mbar). Eventually, the surface was flashed to 900 K and cooled down rapidly, which gives rise to the (1x2) missing row reconstruction, according to previous results [40]. The LEED pattern confirms the presence of the just mentioned periodicity, as can be observed in

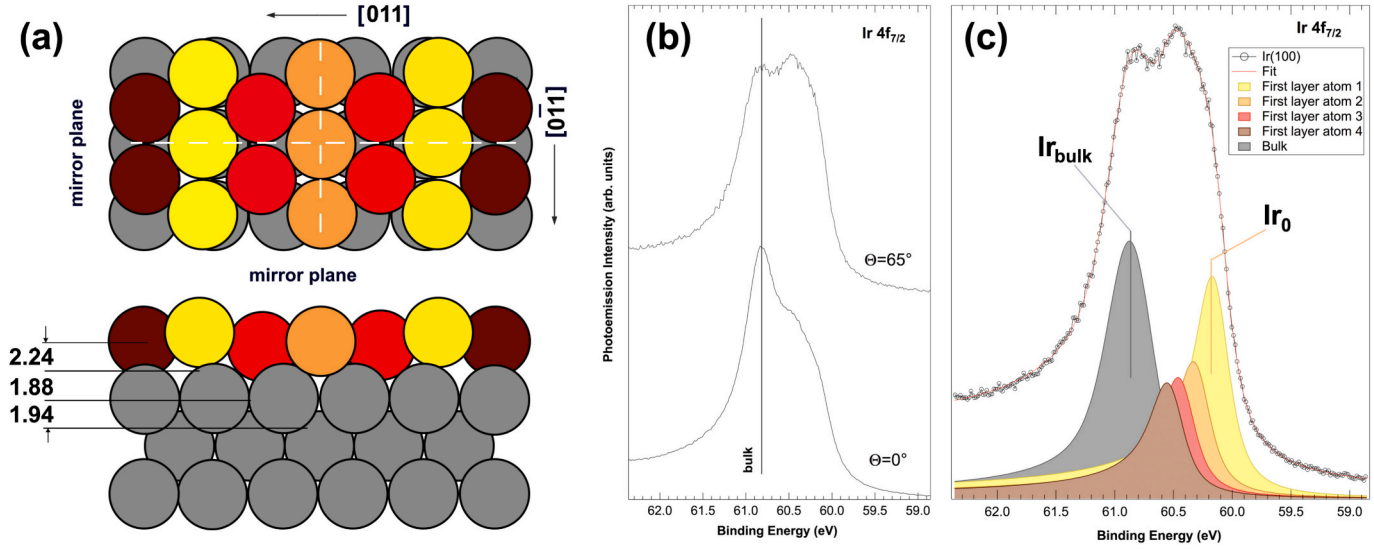

Fig. 3. DFT structure and HR-CLS of Ir(100). (a) Structural geometry as obtained by DFT. The values of inter-layer distances are reported in Å. (b) $4f_{7/2}$ core level spectrum measured at T = 80 K, hv = 185 eV and at two emission angles. (c) $4f_{7/2}$ core level spectra measured at T = 80 K, hv = 185 eV and at grazing emission of 65°. The grey (Ir_{bulk}), yellow (Ir_0), orange, red and brown peaks indicate the bulk and clean surface components, respectively, of the (1x5) quasi-hexagonal structure, while the red curve is the result of the fitting.

Table 2
DFT Computed and experimental core level shifts for Ir(100) surface atoms from this work and from Ref. [39]. Error bars associated to experimental values are ± 30 meV.

	This work		Previous work [42]	
	DFT (meV)	EXP (meV)	DFT (meV)	EXP (meV)
Atom 1	−660	−700	−700	−720
Atom 2	−540	−540	−550	−570
Atom 3	−410	−410	−400	−400
Atom 4	−330	−330	−340	−320

Supplementary Fig. S2. Even though from theoretical calculations higher order reconstructions are less energetically favourable [41], we simulated the unreconstructed (1x1), the reconstructed (1x3), and experimentally observed (1x2) surface, and for all three structures we computed the core levels of each atom. Relaxation results agree with the work of Kaghazchi *et al.* [14], where the unreconstructed (1x1) surface presents the typical contraction of interlayer distance between first and second layers, followed by an oscillatory behaviour of the spacing of inner layers. On the contrary, for the (1x2) and (1x3) periodicity, the contraction of the interlayer distance continues unless the first full atoms layer is created, as shown in Fig. 2(a). The computed core levels of all the reconstructed surfaces are reported in Table 1. The fitting of the Ir (110) spectrum resulted in three surface components shifted by −710 ± 30 meV, −430 ± 30 meV and −140 ± 30 meV from the bulk component (see Fig. 2b), in close agreement with the DFT calculated values corresponding to the (1x2) reconstruction observed by LEED. The bulk component has been found at a binding energy of 60.85 ± 0.02 eV, in agreement with the one of Ir(111). Line shape parameters were similar to those found for (111) surface, with a larger Lorentzian and asymmetry values (0.27 eV and 0.23) for surface atoms with respect to bulk atoms (0.17 eV and 0.13).

3.3. Ir(100)

The reconstruction of Ir(100) causes an increase of atomic density in the topmost layer, resulting in the formation of a quasi-hexagonal atomic arrangement where, along the [011] direction, there is one extra atom, for a total of 6 atoms in a (1x5) cell [41]. This reconstruction is not limited to the surface layer but extends over the first few layers under the surface, with a characteristic buckling of the atoms in all these planes [19]. All surface atoms show a nominal coordination equal to 8, apart from the atom depicted in brown in Fig. 3a, whose coordination is reduced to 7. The average interlayer distances are 2.24 Å, 1.88 Å, and 1.94 Å for $\overline{d}_{12}$, $\overline{d}_{23}$, and $\overline{d}_{34}$, respectively. A more-in-depth insight of the buckling of the atoms is presented in Supplementary Table 1.

The $4f_{7/2}$ spectra reported in Fig. 3(b) show the modification of the photoemission line shape related to measurements at different emission angles (θ being the angle with respect to the surface normal), which result in variable surface sensitivity, due to different electron inelastic mean free path and photoelectron diffraction effects. The fit of high-resolution Ir $4f_{7/2}$ core level spectrum acquired with 185 eV photons is shown in Fig. 3(c). Since the spectrum acquired at normal emission (bottom curve in Fig. 3(b)) is less surface sensitive, we decided to acquire a spectrum at grazing emission (65° out-of-normal) to better disentangle the contributions of all the inequivalent surface atoms. Besides the bulk one, four extra components are needed to accurately fit the spectrum, whose shifts with respect to the bulk are of −700 ± 30 meV, −540 ± 30 meV, −410 ± 30 meV and −330 ± 30 meV. These shifts agree well with the computed core levels previously reported [42], as can be seen from the comparison in Table 2. The larger Gaussian value found for the bulk component, i.e. 0.34 eV, in Ir(100) spectrum, with respect to Ir(110) and Ir(111) (0.20 eV and 0.17 eV, respectively), can be justified by the presence of other components at slightly higher and lower binding energies with respect to 60.84 eV, which we attribute to atoms in the second and third layers.

3.4. Ir(510)

The (5x1) reconstruction of Ir(510), as evidenced by the LEED pattern shown in Supplementary Fig. S3, has been obtained by sputtering and annealing to 1273 K without oxygen treatment. While ideal bulk terminated surface presents 5 atoms on (100) terraces and monoatomic steps oriented along the (110) plane (Fig. 4(a)) the LEED pattern presents bright spots corresponding to the (1x5) reconstruction, as it happens for Ir(100), plus additional spots close to the integer ones which move as a function of electron beam energy with respect to the other spots, thus indicating the presence of steps.

As for the (100) surface the $4f_{7/2}$ photoemission line shape corresponding to different measurements conditions (emission angle θ and photon energy) clearly change giving the opportunity to enhance the surface related components, as reported in Fig. 4(b), facilitating surface

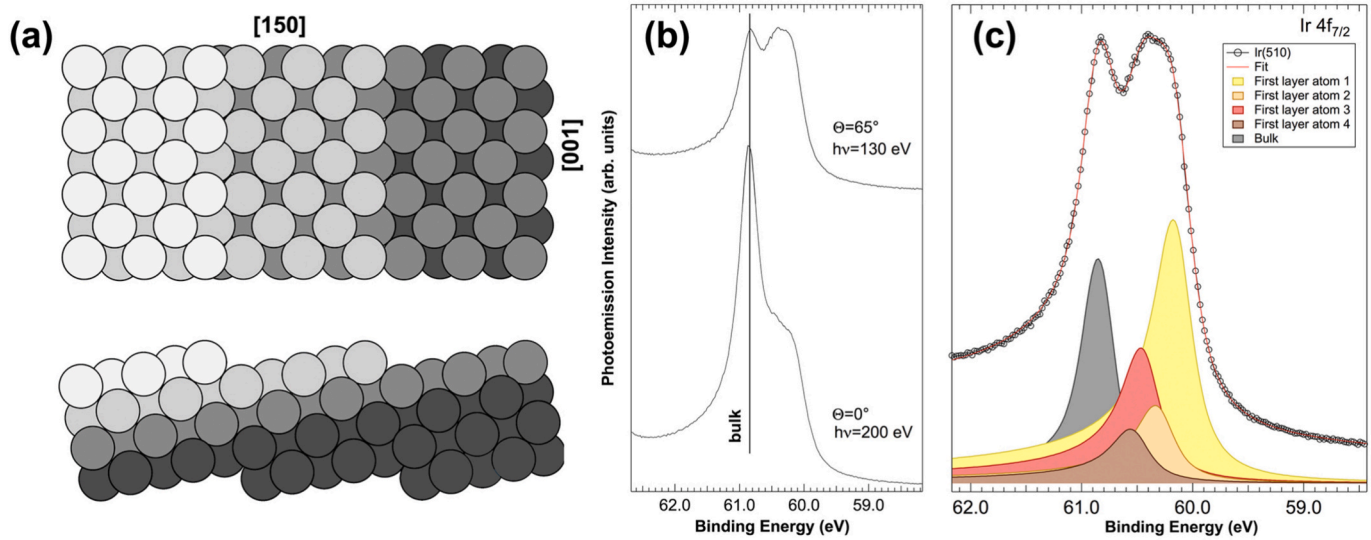

Fig. 4. Structural model of the ideally bulk terminated Ir(510) surface. (b) $4f_{7/2}$ core level spectra measured at T = 80, and at two emission angles and photon energies. (c) $4f_{7/2}$ core level spectrum measured at T = 80 K, hv = 130 eV and at grazing emission of 65°. The grey (Ir_{bulk}), yellow (Ir_0), orange, red and brown peaks indicate the bulk and clean surface components, respectively, while the red curve is the result of the fitting.

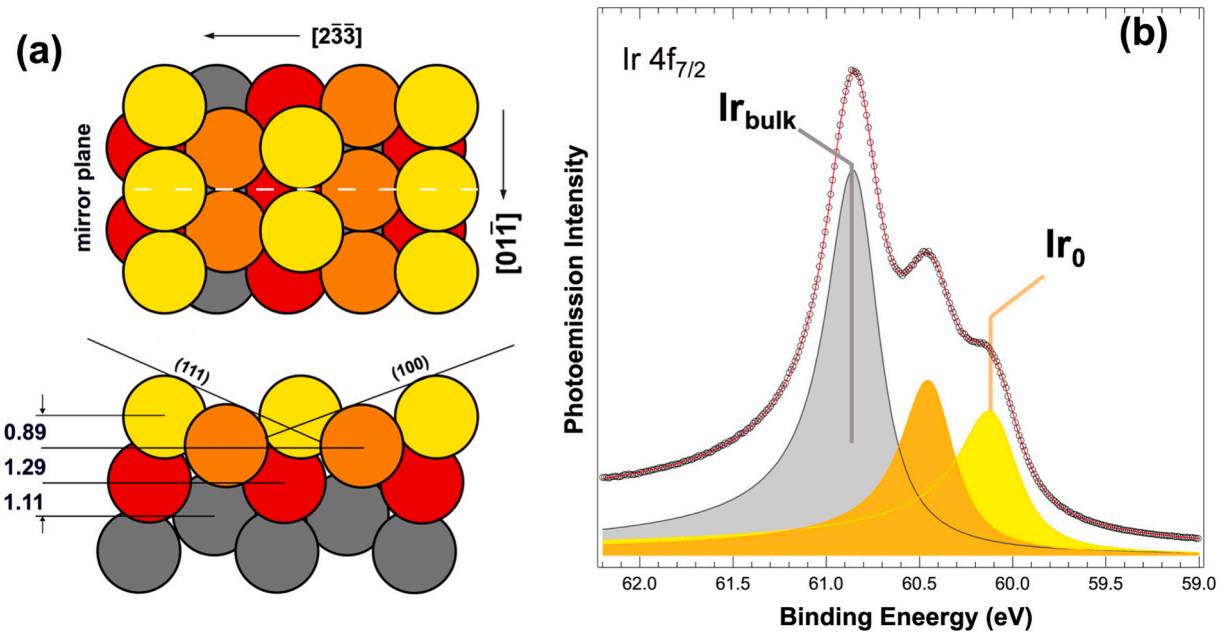

Fig. 5. DFT structure and HR-CLS of Ir(311). (a) DFT structural model. The values of the inter-layer distances are reported in Å. (b) Ir $4f_{7/2}$ core level spectra of clean Ir(311) collected at T = 80 K and $h\nu$ = 200 eV. The gray (Ir_{bulk}), yellow (Ir_0), orange peaks indicate the bulk and clean surface components, respectively, while the red curve is the result of the fitting.

sensitivity. This occurs for example at grazing emission and 130 eV photon energy, as shown in Fig. 4(c), where the Ir $4f_{7/2}$ core level spectrum appears very similar to the one measured for Ir(100), reported in Fig. 3(c). Given that, we decided to fit the Ir $4f_{7/2}$ core level spectrum using the same number of surface components employed for the (100) surface, positioned at the same binding energy. This procedure resulted in a high-quality fit, thus confirming that surface reconstruction similar to the one developed on Ir(100) takes place also on the terraces of Ir (510). We did not add to the fitting any component attributed to atoms on the steps since we expect their coordination to be very similar to some of the atoms in the (100)-(1x5) surface and, thus presenting a similar core-level binding energy shift.

3.5. Ir(311)

After the cleaning procedure with oxygen and hydrogen reported in the Experimental section, the Ir(311) surface exhibited a sharp (1x1) LEED pattern, as shown in Supplementary Fig. S4. Unlike the (311) surface of Pt [43], which shows a (1x2) missing-row reconstruction, LEED suggests that in the case of Ir(311) the surface remains unreconstructed, as for the (311) surface terminations of Au, Ag, Pd [44], Rh, Cu and Ni [45–47]. The unit cell is oblique, with a measured angle between the unit vectors of 73.3°±0.8° (expected value of 73.2°), and a modulus ratio of 1.69 ± 0.04 in agreement with bulk predictions of 1.73.

According to the DFT results, the relaxed structure, reported in Fig. 5 (a), shows the typical alternating contraction and expansion of the inter-layer spacings. More specifically we obtained values of d_{12} = 0.89 Å, d_{23} = 1.29 Å and d_{34} = 1.11 Å, which corresponds to a change of –22.8 %, +11.8 % and −3.7 % with respect to the interplanar values of bulk Ir (d_{bulk} = 1.154 Å). This behavior is consistent with a general trend observed in a number of structural investigations on transition metal surfaces [48].

The high-resolution Ir $4f_{7/2}$ core level spectrum of the clean surface measured at hv = 200 eV and normal emission is shown in Fig. 5(b). Contrary to the Ir(111) surface, that shows only two components separated by 550 meV, the spectrum of the Ir(311) surface clearly presents an additional component, as previously reported in a variety of simple and transition metals, such as the (0001) and (10$\bar{1}$0) [49] Be surfaces or the (0001) [28] and (10$\bar{1}$0) [27] Ru surfaces, indicating the presence of non-equivalent sub-surface atoms with a different electronic structure with respect to the top layer and bulk atoms. The intensity of the lower binding energy component (Ir_0), extracted from a series of spectra measured while exposing the clean surface to oxygen (see Supplementary Fig. S5), clearly diminishes with increasing oxygen adsorption. Based on these considerations we assigned the lower BE component to the first-layer atoms, while the Ir_1 peak in Fig. 5(b) in between is assigned to second–layer atoms. From the fitting procedure, we found a first- and second-layer CLS of − 750 ± 30 meV and −410 ± 30 meV respectively, in agreement with theoretical values of −760 meV and −390 meV. Lorentzian and asymmetry parameters for bulk and surface atoms were found to be equal to 0.22 eV and 0.15, 0.27 eV and 0.23, respectively. It is interesting to note that the best-fit Lorentzian width values for all surfaces were in the range 0.22–0.27. Asymmetry parameters ranging between 0.13 and 0.15 were obtained for second and deeper-layer components as well as for bulk one, i.e. considerably lower than the value of 0.23 found for the first-layer peaks.

4. Discussion

Larger values of Lorentzian and Gaussian broadening, together with asymmetry values, were found for surface components with respect to the bulk ones. This trend has already been reported for a variety of transition metals, including Ta and Rh. An increased Gaussian width can be associated to the expected phonon softening at the surface, which typically results in a lower Debye temperature of top-layer atoms with respect ot the bulk ones [50,51]. The asymmetry parameter instead is linked to the density of states at Fermi level and, thus, to the reactivity of the system, as we will point out later. A higher value of the asymmetry can thus suggest a higher chemical reactivity of surface atoms. Eventually, larger values of Lorentzian broadening, linked to the core–hole lifetime, are associated to an increased probability of Auger transition or other d-excitation processes for surface atoms [52,53].

Our results show an overall agreement between experimentally determined CLS values and DFT calculations for all investigated surfaces. The nominal atomic coordination number of the investigated surface atoms, ranging from 7 to 11, is reflected in the value of the SCLS

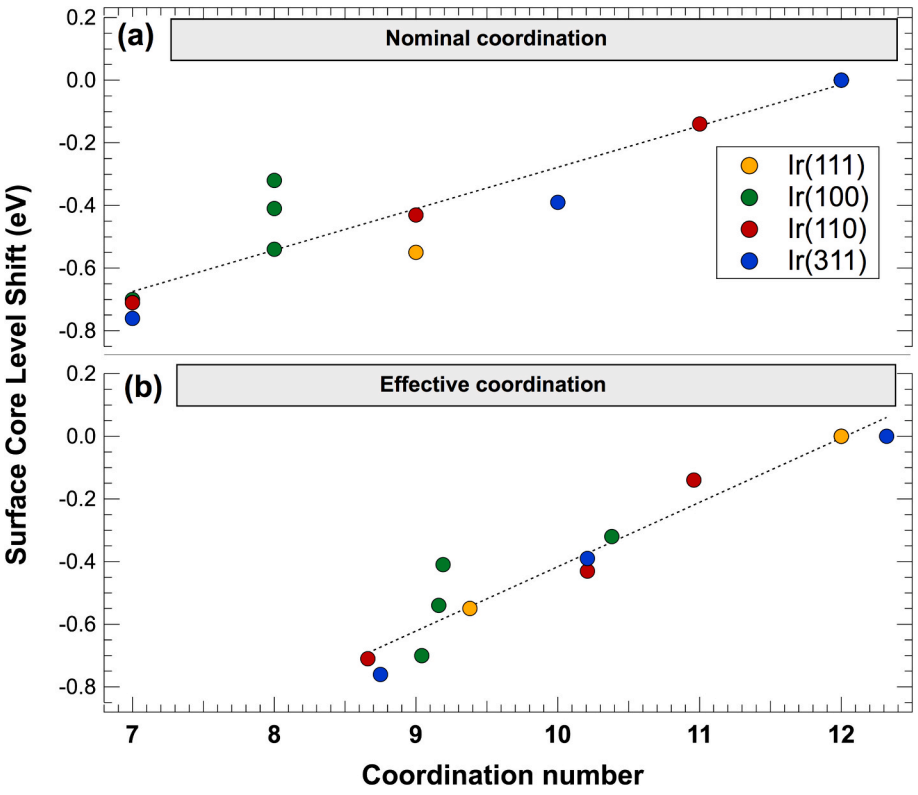

Fig. 6. DFT calculated Surface Core Level Shifts of Ir(111), Ir(100), Ir(110), and Ir(311) as a function of (a) the nominal coordination and (b) the effective coordination.

ranging from −760 meV to −140 meV.

The first layer core level shift of Ir(311) is very similar to the one of Ir (110)-(1x2) and also agrees with core level shift of terrace atoms of Ir (332) [54]. They indeed present the same coordination number, i.e. n = 7. It is worth noting that surface atoms of Ir(210), that show a coordination number equal to 6, have a similar shift (−710 meV) [55]. More surprising is the SCLS of first-layer Ir(100) atoms reported for the metastable Ir(100)-(1x1) surface, even though the expected coordination number is higher and equal to n = 8. However this value is strongly influenced by the first-to-second layer relaxation in Ir(100), for which indeed we found a positive + 100 meV core level shift for the second-layer atoms.

In line with the trend of lower core level shifts for highly coordinated atoms, atoms with coordination equal to 9 present similar SCLS in all the examined surfaces (−450 meV for Ir(210), −430 meV for Ir(110)-(1x2) and −480 meV for Ir(332)), apart from the surface atoms of Ir(111) whose shift has a value of −550 meV. It is worth emphasizing that there are apparent anomalies also in the SCLS of surface atoms of Ir(100)-(1x5) reconstruction. Although they have, in principle, almost all the same nominal coordination, their shifts are spanning in a quite broad interval, ranging from −540 meV to −320 meV. We expect that these huge differences can be explained by taking into account the effective coordination number of those atoms. When comparing the trend in core levels as the local atomic coordination changes, it is necessary indeed to consider local variations in inter-atomic distances, as proposed in the Embedded Atom Model [56–58] for cohesive energies, where the charge density at the atomic site is the result of the contribution of the first neighbors. Since the charge density decays as the nucleus of the interacting atom moves away, the atoms that are closer contribute more to the variations. The expression for the charge density results to be [59]:

$$n_e(\mathrm{i}) = \Sigma_\mathrm{i}[b(R_{bulk}\text{-}R_{ij})] \quad (4)$$

where R_{ij} is the distance of the j nearest-neighbor from the i atom, R_{bulk} is the bulk interatomic distance and b is the decay constant of an isolated Ir atom charge density distribution, which can be fitted with an exponential. The result of considering effective coordination number in place of standard coordination can be seen by comparing Fig. 6(a) and (b).

The trend of SCLS as a function of standard coordination clearly resembles a linear trend ($R^2 = 0.89$). We want to underline that an even better linear trend, based on initial-state effects, is arguably difficult to achieve since the contribution of final-states to the core level shifts, which are included in our calculations, cannot be completely excluded. However, some of the points, belonging to the atoms of Ir(100) and Ir (111), deviate substantially from the linear fit. By considering the effective coordination, these deviations are lowered, and the dependence can be described quite well using a linear relationship, as verified from the increased value of the R^2 coefficient of determination (R^2 = 0.94).

Since less coordinated atoms usually represent catalytic active sites [60], we decided to investigate the correlation between the changes in the projected d-band centroid $\Delta B_d = B^{id}_{surf} - B^{id}_{bulk}$ between bulk and surface atoms, in all the considered surfaces, and the SCLS for the corresponding atoms. The d-band model developed by Hammer and Norskov [61], has been widely used in the past twenty-five years to predict the strength of the bonds between adsorbates and transition metals. In general, stronger bonds are associated with higher energy positions, relative to Fermi Energy, of d-states. The d-band width, and thus the d-band shift, show a substantial dependence on the environment of an atom, particularly on its coordination number. For example, CO chemisorption energy increases by more than 1 eV going from highly coordinated Pt sites, as the ones in Pt(100)-hex reconstructed surfaces, to low coordinated sites as steps and kinks in the vicinal Pt(11,8,5) surface [62]. Even dissociation energies of molecules follow this trend, making the d-band model a useful way to predict the reactivity at surfaces. Lastly, this model can be extended also to transition metal alloys [63] and nanoclusters/nanoparticles [64,65]. In addition, even modification in the local interatomic distance contributes to variations of d-band

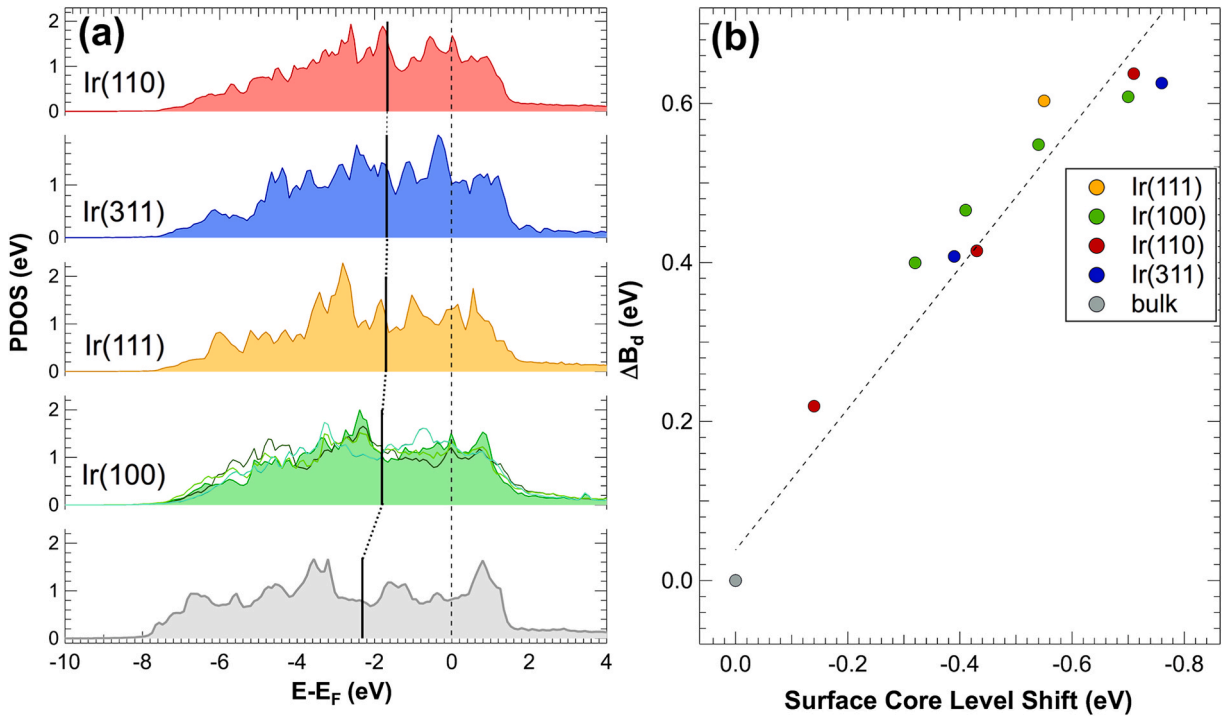

Fig. 7. (a) Density of states projected onto the 5d orbitals of the Ir atoms for all the inequivalent surface atoms of the investigated Ir surfaces. Bottom curve corresponds to Ir bulk atoms. (b) Calculated atom-projected d-band center shift ΔB_d as a function of core level shifts.

centres and thus chemical reactivity. This is the case of strained Ru (0001) that shows larger adsorption energies for CO and O when the surface lattice parameter is increased from 2.70 Å to 2.80 Å [66], and lower N_2 activation energy if the interplanar spacing is enlarged (compressive strain) [67].

We computed the projected density of states per Ir atom for all the Ir surfaces and the d-band centre. In Fig. 7(a), we report the DOS projected onto first-layer Ir atoms of the (100), (111), (311) and (110) and Ir bulk atoms. The effect of reduced coordination results in both (i) a narrowing of the Ir d-band and (ii) an increase of the DOS at the Fermi energy. The latter agrees with the trend of the asymmetry parameter (i.e. lower values for bulk atoms, higher values for surface atoms) that takes into account the probability of excitation of electron-hole pairs and, thus, it is directly related to the density of states at the Fermi level.

The effect of d-band narrowing results in a shift of the projected density of states centre of mass towards the Fermi level, as shown by the thick marks. In Fig. 7(b) we plot the shift of the projected d-band centre ΔB_d versus the calculated SCLS of Ir atoms in the different atomic configurations. The linear dependence between ΔB_d and SCLS reported in Fig. 7(b) suggests that, for the case of Ir, initial state effects in the photoemission process are dominant in the $4f_{7/2}$ core level spectra. The linear relationship between these two quantities shows an almost 1:1 ratio (slope 0.89 ± 0.03), as previously demonstrated also for a large number of (100) surfaces of 4d transition metals [68]. Our findings thus suggest that even in Ir the measured SCLS can be used as a reliable indicator of the local chemical reactivity.

5. Conclusions

In this work, using high-resolution core level photoelectron spectroscopy, we have demonstrated that the Ir $4f_{7/2}$ SCLS measured and calculated for a variety of Ir surfaces can be considered a fingerprint for local chemical coordination and structure. Density Functional Theory calculations confirm that discrepancies in the linear relationship between SCLS and coordination number originate in the variations of the local interatomic distances. Besides this trend, we were able to correlate the d-band centroid shifts with SCLS, thus confirming that, also for Ir, SCLS can be considered as a good descriptor of the local chemical reactivity of Ir surfaces.

CRediT authorship contribution statement

Deborah Perco: Writing – original draft, Investigation, Formal analysis, Data curation. **Monica Pozzo:** Writing – review & editing, Investigation, Formal analysis. **Andrea Berti:** Writing – review & editing, Investigation. **Paolo Lacovig:** Writing – review & editing, Investigation. **Marco Bianchi:** Writing – review & editing, Investigation. **Silvano Lizzit:** Writing – review & editing, Investigation. **Dario Alfè:** Writing – review & editing, Funding acquisition, Formal analysis. **Alessandro Baraldi:** Writing – original draft, Supervision, Investigation, Funding acquisition, Conceptualization.

Declaration of competing interest

The authors declare that they have no known competing financial interests or personal relationships that could have appeared to influence the work reported in this paper.

Acknowledgments

A.B. and D.A. acknowledge MUR for the support of the PRIN Project no. 20222FXZ33 entitled “Materials modelling for energy storage applications”. This work used the ARCHER2 UK National Supercomputing Service (https:// www.archer2.ac.UK). We acknowledge Elettra Sincrotrone Trieste for providing access to its synchrotron radiation facilities and for financial support.

Appendix A. Supplementary data

Supplementary data to this article can be found online at https://doi.org/10.1016/j.apsusc.2025.163294.

Data availability

Data will be made available on request.

References

[1] A.R. Poerwoprajitno, L. Gloag, S. Cheong, J.J. Gooding, R.D. Tilley, Synthesis of low- and high-index faceted metal (Pt, Pd, Ru, Ir, Rh) nanoparticles for improved activity and stability in electrocatalysis, Nanoscale 11 (2019) 18995, https://doi.org/10.1039/C9NR05802H.

[2] G. Collins, M. Schmidt, C. Odwyer, G. McGlacken, J.D. Holmes, Enhanced catalytic activity of high-index faceted palladium nanoparticles in suzuki-miyaura coupling due to efficient leaching mechanism, ACS Catal. 4 (2014) 3105–3111, https://doi.org/10.1021/cs5008014.

[3] L. Huang, M. Liu, H. Lin, Y. Xu, J. Wu, V.P. Dravid, C. Wolverton, C.A. Mirkin, Shape regulation of high-index facet nanoparticles by dealloying, Science 365 (2019) 1159–1163, https://doi.org/10.1126/science.aax5843.

[4] Y. Li, H. Lin, W. Zhou, L. Sun, D. Samanta, C.A. Mirkin, Corner-, edge-, and facet-controlled growth of nanocrystals, Sci. Adv. 7 (2021) 1–6, https://doi.org/10.1126/sciadv.abf1410.

[5] X. Chen, C. Li, B. Li, Y. Ying, S. Ye, D.N. Zakharov, S. Hwang, J. Fang, G. Wang, Y. J. Hu, G. Zhou, Surface self-diffusion induced sintering of nanoparticles, ACS Nano 18 (2024) 31160–31173, https://doi.org/10.1021/acsnano.4c09056.

[6] J. Junnan, C. Shuffen, Z. Yin, S. Guangbin, J. Junhui, Z. Xiaoqin, C. Mingwei, L. Pan, Crystal plane orientation-dependent surface atom diffusion in sub–10-nm Au nanocrystals, Sci. Adv. 10 (2024) 21, https://doi.org/10.1126/sciadv.adn5946.

[7] L. Xu, K.G. Papanikolaou, B.A.J. Lechner, L. Je, G.A. Somorjai, M. Salmeron, M. Mavrikakis, Formation of active sites on transition metals through reaction-driven migration of surface atoms, Science 380 (2023) 70–76, https://doi.org/10.1126/science.add0089.

[8] A. Baraldi, Structure and chemical reactivity of transition metal surfaces as probed by synchrotron radiation core-level photoelectron spectroscopy, J. Phys.: Condens. Matter 20 (2008) 93001, https://doi.org/10.1088/0953-8984/20/9/093001.

[9] L. Bianchettin, A. Baraldi, S. de Gironcoli, E. Vesselli, S. Lizzit, L. Petaccia, G. Comelli, R. Rosei, Core level shifts of undercoordinated Pt atoms, J. Chem. Phys. 128 (2008) 11, https://doi.org/10.1063/1.2841468.

[10] T. Dinh, Z. Dobo, H. Kovacs, Phytomining of noble metals – A review, Chemosphere 286 (2022) 131805, https://doi.org/10.1016/j.chemosphere.2021.131805.

[11] T. Reier, M. Oezaslan, P. Strasser, Electrocatalytic oxygen evolution reaction (OER) on Ru Ir, and Pt catalysts: A comparative study of nanoparticles and bulk materials,, ACS Catal. 2 (2012) 1765–1772, https://doi.org/10.1021/cs3003098.

[12] J. Quinson, Iridium and IrO_x nanoparticles: an overview and review of syntheses and applications, Adv. Colloid Interfac. 303 (2022) 102643, https://doi.org/10.1016/j.cis.2022.102643.

[13] J. Coraux, A.T. N'Diaye, M. Engler, C. Busse, D. Wall, N. Buckanie, F.J. Meyer zu Heringdorf, R. Van Gastel, B. Poelsema, T. Michely, Growth of graphene on Ir (111), New J. Phys. 11 (2009) 023006, https://doi.org/10.1088/1367-2630/11/2/023006.

[14] P. Kaghazchi, T. Jacob, First-principles studies on clean and oxygen-adsorbed Ir (110) surfaces, Phys. Rev. B 76 (2007) 245425, https://doi.org/10.1103/PhysRevB.76.245425.

[15] J. Kuntze, J. Bomermann, T. Rauch, S. Speller, W. Heiland, Surface reconstruction of the Ir(110) surface, Surf. Sci. 394 (1997) 150–158, https://doi.org/10.1016/S0039-6028(97)00602-X.

[16] J. Grant, A LEED study of the Ir(100) surface, Surf. Sci. 18 (1968) 228, https://doi.org/10.1016/0039-6028(69)90167-8.

[17] M. Van Hove, R. Koestner, P. Stair, J. Biberian, L. Kesmodel, I. Bartos, J. Somorjai, The surface reconstructions of the (100) crystal faces of iridium, platinum and gold. II. structural determination by LEED intensity analysis, Surf. Sci. 103 (1981) 218, https://doi.org/10.1016/0039-6028(81)90108-4.

[18] N. Bickel, K. Heinz, Quasidynamical LEED structure determination of the Ir(100) 1×5 surface reconstruction, Surf. Sci. 163 (1985) 435–443, https://doi.org/10.1016/0039-6028(85)91070-2.

[19] Q. Ge, D. King, N. Marzari, N. Payne, First principles calculation of the energy and structure of two solid surface phases on Ir(100), Surf. Sci. 418 (1998) 529–535, https://doi.org/10.1016/S0039-6028(98)00764-X.

[20] A. Schmidt, W. Meier, L. Hammer, K. Heinz, Deep-going reconstruction of Ir(100)-5x1, J. Phys.: Condens. Matt. 14 (2002) 12353–12365, https://doi.org/10.1088/0953-8984/14/47/310.

[21] P. Kaghazchi, T. Jacob, I. Ermanoski, W. Chen, T.E. Madey, First-principles studies on oxygen-induced faceting of Ir(210), ACS Nano 2 (2008) 1280–1288, https://doi.org/10.1021/nn800210v.

[22] V. Pfeifer, T.E. Jones, J.J. Velasco Vélez, C. Massué, R. Arrigo, D. Teschner, F. Girgsdies, M. Scherzer, M.T. Greiner, J. Allan, M. Hashagen, G. Weinberg, S. Piccinin, M. Hävecker, A. Knop-Gericke, R. Schlögl, The electronic structure of iridium and its oxides, Surf. Interface Anal. 48 (2016) 261–273, https://doi.org/10.1002/sia.5895.

[23] H.G. Sanchezcasalongue, M.L. Ng, S. Kaya, D. Friebel, H. Ogasawara, A. Nilsson, In Situ observation of surface species on iridium oxide nanoparticles during the oxygen evolution reaction, Angew. Chem. Int. Edit. 53 (2014) 7169–7172, https://doi.org/10.1002/anie.201402311.

[24] D.C. Madden, M.L. Bentley, S.J. Jenkins, S.M. Driver, On the role of molecular chirality in amino acid self-organisation on Cu{311}, Surf. Sci. 629 (2014) 81–87, https://doi.org/10.1016/j.susc.2014.03.025.

[25] C.A. de Wolf, M.O. Hattink, B.E. Nieuwenhuys, Oscillatory behaviour in the NO–H_2 reaction over Ir(510), Surf. Sci. 471 (2001) 114–124, https://doi.org/10.1016/S0039-6028(00)00900-6.

[26] A. Baraldi, V.R. Dhanak, Design study of a double pass hemispherical electron energy analyser with multichannel detection, J. Electron Spectrosc. 67 (1994) 211–220, https://doi.org/10.1016/0368-2048(93)02038-N.

[27] A. Baraldi, S. Lizzit, G. Comelli, A. Goldoni, P. Hofmann e G. Paolucci, Core-level subsurface shifted component in a 4d transition metal: Ru(10$\bar{1}$0), Phys. Rev. B 61 (2000) 4534 https://doi.org/10.1103/PhysRevB.61.4534.

[28] S. Lizzit, A. Baraldi, A. Groso, K. Reuter, M.V. Ganduglia-Pirovano, C. Stampfl, M. Scheffler, M. Stichler, C. Keller, W. Wurth, D. Menzel, Surface core-level shifts of clean and oxygen-covered Ru(0001), Phys. Rev. B 63 (2001) 205419, https://doi.org/10.1103/PhysRevB.63.205419.

[29] A. Baraldi, S. Lizzit, G. Comelli, G. Paolucci, Oxygen adsorption and ordering on Ru (10$\bar{1}$0), Phys. Rev. B 63 (2001) 115410, https://doi.org/10.1103/PhysRevB.63.115410.

[30] S. Doniach, M. Sunjic, Many-electron singularity in X-ray photoemission and X-ray line spectra from metals, J. Phys. C: Solid State Phys. 3 (1970) 285, https://doi.org/10.1088/0022-3719/3/2/010.

[31] A. Baraldi, S. Lizzit, A. Novello, G. Comelli, R. Rosei, Second-layer surface core-level shift on Rh(111), Phys. Rev. B 67 (2003) 205404, https://doi.org/10.1103/PhysRevB.67.205404.

[32] M. Bianchi, D. Cassese, A. Cavallin, R. Comin, F. Orlando, L. Postregna, E. Golfetto, S. Lizzit, A. Baraldi, Surface core level shifts of clean and oxygen covered Ir(111), New J. Phys. 11 (2009) 063002, https://doi.org/10.1088/1367-2630/11/6/063002.

[33] I. Hamada, Van der Waals density functional made accurate, Phys. Rev. B 89 (2014) 121103, https://doi.org/10.1103/PhysRevB.89.121103.

[34] G. Kresse, Efficient iterative schemes for ab initio total-energy calculations using a plane-wave basis set, Phys. Rev. B 54 (1996) 11169, https://doi.org/10.1103/PhysRevB.54.11169.

[35] B. Johansson, N. Martensson, Core-level binding-energy shifts for the metallic elements, Phys. Rev. B 21 (1980) 4427, https://doi.org/10.1103/PhysRevB.21.4427.

[36] P. Lacovig, M. Pozzo, D. Alfe, P. Vilmercati, A. Baraldi, S. Lizzit, Growth of dome-shaped carbon nanoislands on Ir(111): The intermediate between carbidic clusters and quasi-free-standing graphene, Phys. Rev. Lett. 103 (2009) 166101, https://doi.org/10.1103/PhysRevLett.103.166101.

[37] R. Koch, M. Borbonus, O. Haase, K.H. Rieder, New aspects on the Ir(110) reconstruction: Surface stabilization on mesoscopic scale via (331) facets, Phys. Rev. Lett. 67 (1991) 3416, https://doi.org/10.1103/PhysRevLett.67.3416.

[38] S.M. Foiles, Reconstruction of fcc(110) surfaces, Surf. Sci. 191 (1987) L779–L786, https://doi.org/10.1016/S0039-6028(87)81038-5.

[39] W. Moritz, D. Wolf, Structure determination of the reconstructed Au(110) surface, Surf. Sci. 88 (1979) L29–L34, https://doi.org/10.1016/0039-6028(79)90093-1.

[40] J.J. Schultz, M. Sturmat e R. Koch, Illuminating structural transformation of Ir (110): A high-temperature scanning tunneling microscopy study, Phys. Rev. B 62 (2000) 23 https://doi.org/10.1103/PhysRevB.62.15402.

[41] A. Filippetti, V. Fiorentini, Reconstructions of Ir(110) and (100): an ab initio study, Surf. Sci. 1 (1997) 112–116, https://doi.org/10.1016/S0039-6028(96)01374-X.

[42] M.A. Arman, A. Klein, P. Ferstl, A. Valookaran, J. Gustafson, K. Schulte, E. Lundgren, K. Heinz, A. Schneider, F. Mittendorfer, L. Hammer, J. Knudsen, Adsorption of hydrogen on stable and metastable Ir(100) surfaces, Surf. Sci. 656 (2017) 66–76, https://doi.org/10.1016/j.susc.2016.10.002.

[43] H. Orita, Y. Inada, DFT investigation of CO adsorption on Pt(211) and Pt(311) surfaces from low to high coverage, J. Phys. Chem. B 109 (2005) 22469–22475, https://doi.org/10.1021/jp052583a.

[44] J. Zhang, X. Zhang, Z. Wang, Z. Diao, Adsorption of carbon monoxide on Pd(311) and (211) surfaces, Surf. Sci. 254 (2008) 6327–6331, https://doi.org/10.1016/j.apsusc.2008.03.063.

[45] D.L. Adams, Multilayer relaxation of the Ni(311) surface: a new LEED analysis, Surf. Sci. 149 (1985) 407–422, https://doi.org/10.1016/0039-6028(85)90072-X.

[46] J.M. Zhang, H.Y. Li, K.W. Xu, Missing row reconstructed (110), (211) and (311) surfaces for FCC transition metals, Surf. Interface Anal. 39 (2007) 660–664, https://doi.org/10.1002/sia.2574.

[47] F.H. Tian, Z.X. Wang, Adsorption of an O Atom on the Cu(311) Step Defective Surface, J. Phys. Chem. B 108 (2004) 1392–1395, https://doi.org/10.1021/jp036141f.

[48] M.A. Van Hove, W.H. Weinberg, C.-M. Chan, Low-energy electron diffraction, first ed., Springer, Berlin, Heidelberg, 1986.

[49] J.H. Cho, K.S. Kim, S.H. Lee, M.H. Kang, Z. Zhang, Origin of contrasting surface core-level shifts at the Be(10$\bar{1}$0) and Mg(10$\bar{1}$0) surfaces, Phys. Rev. B 61 (2000) 9975, https://doi.org/10.1103/PhysRevB.61.9975.

[50] E. Ferrari, L. Galli, E. Miniussi, M. Morri, M. Panighel, M. Ricci, P. Lacovig, S. Lizzit, A. Baraldi, Layer-dependent Debye temperature and thermal expansion of Ru(0001) by means of high-energy resolution core-level photoelectron spectroscopy, Phys. Rev. B 82 (2010) 195420, https://doi.org/10.1103/PhysRevB.82.195420.

[51] S.C. Santucci, A. Goldoni, R. Larciprete, S. Lizzit, M. Bertolo, A. Baraldi, C. Masciovecchio, Calorimetry at surface using high-resolution core-level photoemission, Phys. Rev. Lett. 93 (2004) 106105, https://doi.org/10.1103/PhysRevLett.93.106105.

[52] D.M. Riffe, W. Hale, B. Kim, J.L. Erskine, Conduction-electron screening in the bulk and at low-index surfaces of Ta metal, Phys. Rev. B 51 (1995) 11012, https://doi.org/10.1103/PhysRevB.51.11012.
[53] M. Zacchigna, C. Astaldi, K.C. Prince, M. Sastry, C. Comicioli, M. Evans, R. Rosei, C. Quaresima, C. Ottaviani, C. Crotti, M. Matteucci, P. Perfetti, Surface-induced broadening of photoemission core levels, Phys. Rev. B 54 (1996) 7713, https://doi.org/10.1103/PhysRevB.54.7713.
[54] J.F. van der Veen, D.E. Eastman, Intrinsic step-related surface states and 4f-core levels on Ir(332), Solid State Commun. 39 (1981) 1301–1304, https://doi.org/10.1016/0038-1098(81)90231-3.
[55] M.J. Gladys, I. Ermanoski, G. Jackson, J.S. Quinton, J.E. Rowe, T.E. Madey, A high resolution photoemission study of surface core-level shifts in clean and oxygen-covered Ir(210) surfaces, J. Electron Spectrosc. 135 (2004) 105–112, https://doi.org/10.1016/j.elspec.2004.02.109.
[56] M.S. Daw, M.I. Baskes, Semiempirical, quantum mechanical calculation of hydrogen embrittlement in metals, Phys. Rev. Lett. 50 (1983) 1285, https://doi.org/10.1103/PhysRevLett.50.1285.
[57] M.S. Daw, M.I. Baskes, Embedded-atom method: Derivation and application to impurities, surfaces, and other defects in metals, Phys. Rev. B 29 (1984) 6443, https://doi.org/10.1103/PhysRevB.29.6443.
[58] M.S. Foiles, M.I. Baskes, Embedded-atom-method functions for the fcc metals Cu, Ag, Au, Ni, Pd, Pt, and their alloys, Phys. Rev. B 33 (1986) 7983, https://doi.org/10.1103/PhysRevB.33.7983.
[59] A. Baraldi, L. Bianchettin, E. Vesselli, S. de Gironcoli, S. Lizzit, L. Petaccia, G. Zampieri, G. Comelli, R. Rosei, Highly under-coordinated atoms at Rh surfaces: interplay of strain and coordination effects on core level shift, New J. Phys. 9 (2007) 143, https://doi.org/10.1088/1367-2630/9/5/143.
[60] F.B. de Mongeot, A. Toma, A. Molle, S. Lizzit, L. Petaccia, A. Baraldi, Carbon monoxide dissociation on Rh nanopyramids, Phys. Rev. Lett. 97 (2006) 056103, https://doi.org/10.1103/PhysRevLett.97.056103.
[61] J.K. NΦrskov, F. Abild-Pedersen, F. Studt, T. Bligaard, Density functional theory in surface chemistry and catalysis, Proc. Natl. Acad. Sci. 108 (2011) 3, https://doi.org/10.1073/pnas.1006652108.
[62] B. Hammer, O.H. Nielsen, J.K. Norskov, Structure sensitivity in adsorption: CO interaction with stepped and reconstructed Pt surfaces, Catal. Lett. 46 (1997) 31–35, https://doi.org/10.1023/A:1019073208575.
[63] H. Xin, A. Vojvodic, J. Voss, J.K. Norskov, F. Abild-Pedersen, Effects of d-band shape on the surface reactivity of transition metal alloys, Phys. Rev. B 89 (2014) 115114, https://doi.org/10.1103/PhysRevB.89.115114.
[64] Q. Hu, K. Gao, X. Wang, H. Zheng, J. Cao, L. Mi, Q. Huo, H. Yang, J. Liu, C. He, Subnanometric Ru clusters with upshifted d band center to improve performance for alkaline hydrogen evolution reaction, Nat. Commun. 13 (2022) 3958, https://doi.org/10.1038/s41467-022-31660-2.
[65] E. Toyoda, R. Jinnouchi, T. Hatanaka, Y. Morimoto, K. Mitsuhara, A. Visikovskiy, Y. Kido, The d-band structure of Pt nanoclusters correlated with the catalytic activity for an oxygen reduction reaction, J. Phys. Chem. C 115 (2011) 21236–21240, https://doi.org/10.1021/jp206360e.
[66] M. Mavrikakis, B. Hammer, J.K. Korskov, Effect of strain on the reactivity of metal surfaces, Phys. Rev. Lett. 81 (1998) 13, https://doi.org/10.1103/PhysRevLett.81.2819.
[67] T. Xie, J. Zhou, L. Cai, W. Hu, B. Huang, D. Yuan, Synergistic effects of crystal phase and strain for N2 dissociation on Ru(0001) surfaces with multilayered hexagonal close-packed structures, ACS Omega 7 (2022) 4492–4500, https://doi.org/10.1021/acsomega.1c06400.
[68] M.V. Ganduglia-Pirovano, V. Natoli, M.H. Cohen, J. Kudrnovsky, I. Turek, Potential, core-level, and d band shifts at transition-metal surfaces, Phys. Rev. B 54 (1996) 12, https://doi.org/10.1103/PhysRevB.54.8892.